

# *Control Method of Flying Capacitor Converter Operated in Discontinuous Current Mode for High Voltage Photovoltaic Cell*

Jun-ichi Itoh, Ryoichi Ishibashi, Keisuke Kusaka  
Dept. of Electrical Electronics and Information Engineering  
Nagaoka University of Technology  
Niigata, Japan  
itoh@vos.nagaokaut.ac.jp

**Abstract**— This paper proposes the operation method of DCM applied to inductor current control of a flying capacitor converter (FCC) for the low boost ratio. Due to the charging and discharging of the flying capacitor, the inductor current ripple in FCC is reduced compared to that of the typical boost converter with the same inductance. The operation analysis for high boost ratio have been applied by authors. However, the duty calculation for light load region of high boost ratio cannot be applied because the slope of the modes II and III are inverted when boost ratio is less than 2. Thus, the operation analysis for low boost ratio is proposed in this paper. The validity of the proposed method is confirmed with a 1-kW prototype. As the experimental results, an efficiency of 98.1% is achieved.

**Keywords**—*Discontinuous Current Mode; Flying Capacitor Converter;*

## I. INTRODUCTION

In recent years, photovoltaic power generation systems have attracted attention as renewable power sources [1–5]. In general, converter topologies for these systems consists of a boost circuit and a grid-tied inverter. Particularly, it is necessary to install the converter in various places including each household when a photovoltaic power generation system is incorporated in a DC micro grid. Therefore, high power density and high efficiency are required for these power converters. In particular, the boost inductor in the boost converter occupies a large volume in the system. Therefore, miniaturization of this boost inductor is strongly demanded [6].

One of the ideas to downsize the boost inductor is an increase in the switching frequency [7]. However, the effect on the miniaturization of a system by the high switching frequency is limited because the operation in the high-switching frequency leads an increase of switching loss [8].

Other ideas for downsizing the boost inductor is applying discontinuous current mode (DCM) to an inductor current control [9–12]. DCM reduces the inductor volume because the required inductance in DCM is smaller than continuous current mode (CCM). However, a large current ripple occurs as compared with CCM in the trade-off of a small inductor when

DCM is applied to the boost converter. This high-current ripple significantly increases the conduction loss in the switching devices. Hence, the effect on the miniaturization of a system by the DCM operation in the boost converter is restricted.

The inductor current control method with DCM for a three-level FCC has been proposed in order to increase the power density of a DC-DC converter [13]. The proposed control operates FCC using four modes; two of which are the same as these of the boost converter (modes I and IV), whereas the other two modes are charging and discharging modes of the flying capacitor (modes II and III). In this method, the modes II and III inserted between the modes I and IV. This method makes the inductor current waveform trapezoidal shape in heavy load region due to the charging and discharging of the flying capacitor. The conduction loss and the turn-off loss are reduced, because the peak of the inductor current is reduced by this method. However, the control method is taking into account only the operation with a boost ratio more than two.

In this paper, the operation method of low boost ratio is proposed to increase the practicality of this method. The slope of the modes II and III are inverted when the boost ratio become less than two by the flying capacitor voltage and input and output voltage. Therefore, the originality of this paper is the operation analysis for heavy load and light load region in low boost ratio of less than 2. The control based on the analysis was implemented in DSP and confirmed with a prototype.

This paper is organized as follows; firstly, the operation modes of FCC on applying DCM method is introduced. Secondly, the duty calculation method is introduced. Next, the control method for flying capacitor voltage is introduced. Finally, experiments are conducted in order to confirm the circuit operation.

## II. OPERATION MODES OF FLYING CAPACITOR CONVERTER

Figure 1 shows FCC. In this paper, DCM and CRM are applied to FCC in order to reduce the boost inductor current ripple, decreasing the RMS current value against the average current value. Furthermore, since the required inductance value by applying DCM is reduced, the size of the inductor is

downsized. Therefore, both high efficiency and miniaturization are achieved with the proposed method.

Figure 2 shows the operation modes of FCC with applying DCM for inductor current. In the proposed method, the current  $i_L$  flowing through the inductor  $L$  is controlled using four modes; Mode I to VI. In the mode I, energy is stored in  $L$  by turning on  $S_3$  and  $S_4$ . In the mode II and mode III, the energy is stored or released in  $C_{fc}$ . In the mode I and IV, the energy stored in  $L$  is stored or released to the output side by turning on  $S_1$  and  $S_2$ .

#### 1) Mode I

In the mode I, energy is stored in  $L$  by turning on  $S_3$  and  $S_4$ . The slope  $a_1$  of the inductor current in this mode is expressed as

$$a_1 = \frac{v_{in}}{L} \quad (1),$$

where  $v_{in}$  is the input voltage, and  $L$  is the inductance value of the boost inductor.

#### 2) Mode II

In the mode II, the energy is stored in  $C_{fc}$  by turning on  $S_2$  and  $S_4$ . The slope  $a_2$  of the inductor current in this mode is expressed as

$$a_2 = \frac{v_{in} - v_{fc}}{L} \quad (2),$$

where  $v_{fc}$  is the voltage of the flying capacitor  $C_{fc}$ .

#### 3) Mode III

In the mode III, by turning on  $S_1$  and  $S_3$ , the energy stored in  $C_{fc}$  and  $L$  is released to the output side  $v_{dc}$ . The slope  $a_3$  of the inductor current in this mode is expressed as

$$a_3 = \frac{v_{in} - (v_{dc} - v_{fc})}{L} \quad (3),$$

where  $v_{dc}$  is output voltage.

#### 4) Mode IV

In the mode IV, by turning on  $S_1$  and  $S_2$ , the energy stored in  $L$  is released to the output side. The slope  $a_4$  of the inductor current in this mode is expressed as

$$a_4 = \frac{v_{in} - v_{dc}}{L} \quad (4).$$

Figure 3 shows the inductor current waveform in each switching mode during one switching cycle in heavy load region. This control method is obtained by adding the modes II and III to the operation modes of the boost converter with the modes I and IV. Consequently, the inductor current  $i_L$  becomes a trapezoidal waveform.

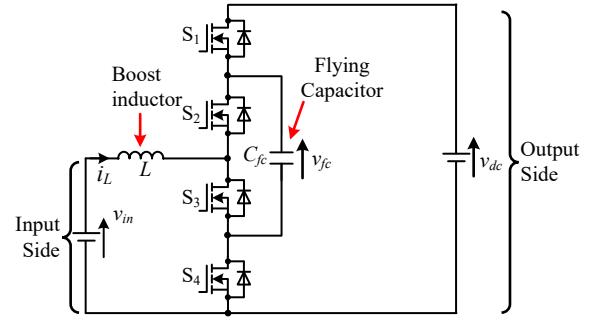


Fig. 1. Three-level flying capacitor converter.

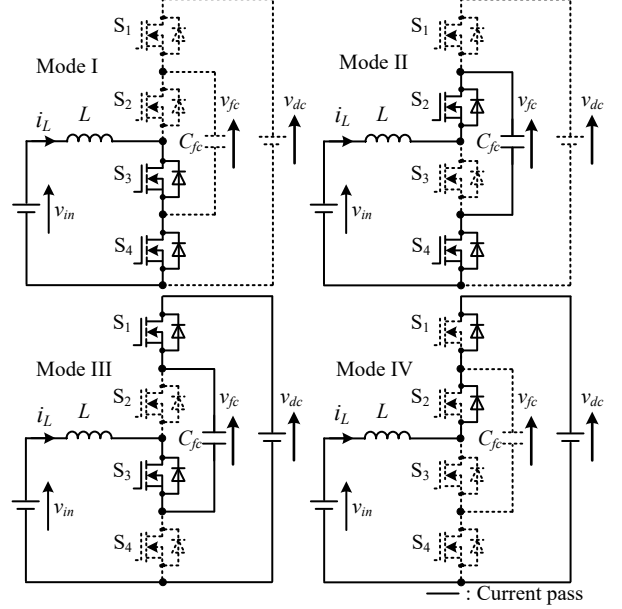


Fig. 2. Operation modes of flying capacitor converter.

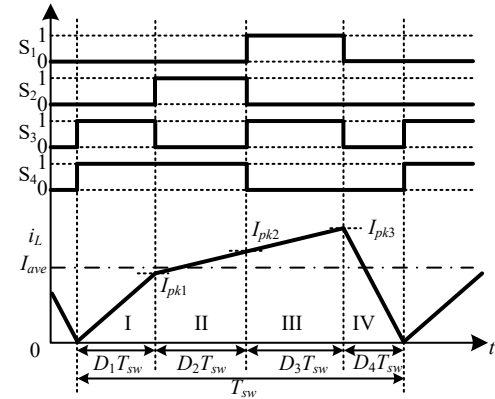


Fig. 3. Inductor current waveform and gate signals of MOSFETs of FCC in rated power for heavy load region.

### III. THE INDUCTOR CURRENT CONTROL WITH DISCONTINUOUS-CURRENT-MODE

#### A. Heavy load region

Figure 4 shows the current waveform variation of each load when the voltage condition and circuit parameters are as an example. In Fig. 4(a), the duty ratio of the modes II and III

become less than zero when the input current is increased. Therefore, the input current is the maximum that can be output under that circuit condition. The other hands, in Fig. 4(c), the duty ratio of Mode II and III become less than zero when the input current is decreased. Therefore, the input current is the minimum that can be output under that circuit condition. This load region, that the input current is trapezoidal waveform, is called ‘‘Heavy load region’’. The slope of the current waveform on each mode depends on the voltage conditions and the circuit parameters. Therefore, the analysis of minimum input current and maximum input current are required in this load region.

The duty ratios in heavy load are expressed as following equations [13].

$$D_1 = -\frac{2v_{in}}{v_{dc}} + 1 + D_4 \quad (5),$$

$$D_2 = \frac{-B + \sqrt{B^2 - 4AC}}{2A} \quad (6),$$

$$D_3 = D_{23} - D_2 \quad (7),$$

$$D_4 = \frac{v_{in} - \sqrt{-v_{in}^2 + v_{in}v_{dc} - 2I_{ave}Lf_{sw}v_{dc}}}{v_{dc}} \quad (8),$$

where  $f_{sw}$  is switching frequency,  $I_{ave}$  is the average input current, A, B, and C are defined following equations

$$\begin{cases} D_{23} = 1 - D_1 - D_4 \\ A = 2\left(v_{in} - \frac{v_{dc}}{2}\right) \\ B = 3v_{in}D_1 - \left(v_{in} - \frac{v_{dc}}{2}\right)D_{23} - (v_{in} - v_{dc})D_4 \\ C = \left\{-v_{in}D_1 + \left(v_{in} - v_{dc}\right)D_4\right\}D_{23} \end{cases} \quad (9).$$

Figure 5 shows the relationship among the duties and average current on the boost inductor. The average current in Fig. 5 is standardized by

$$I_{ave\_pu} = \frac{2LI_{ave}f_{sw}v_{out}}{v_{in}(v_{dc} - v_{in})} \quad (10).$$

Point ‘‘A’’ of Fig. 5 corresponds to Fig. 4(a). Similarly, Point ‘‘B’’ of Fig. 5 corresponds to Fig. 4(c). The input current is limited between A to B of Fig. 5.

The input average current  $I_{ave}$  has an upper limit and a lower limit because all of the duties must be positive although the slope

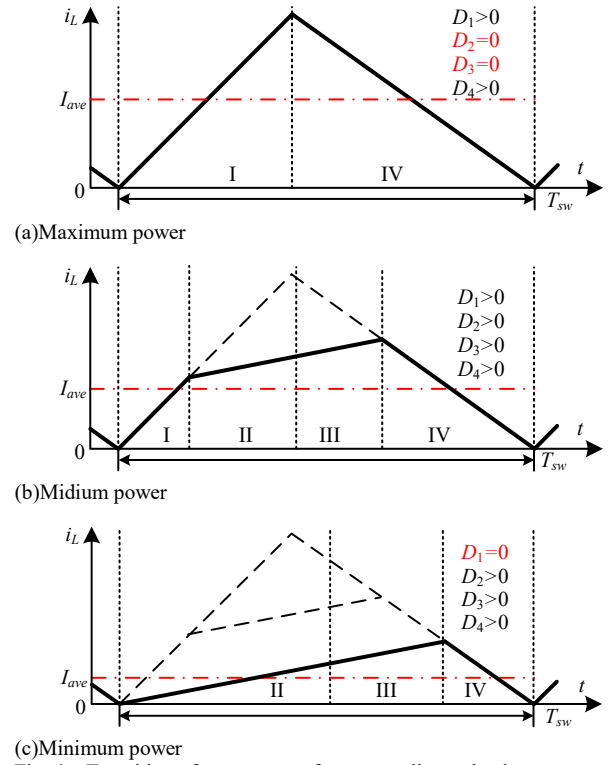


Fig. 4. Transition of current waveform according to load.

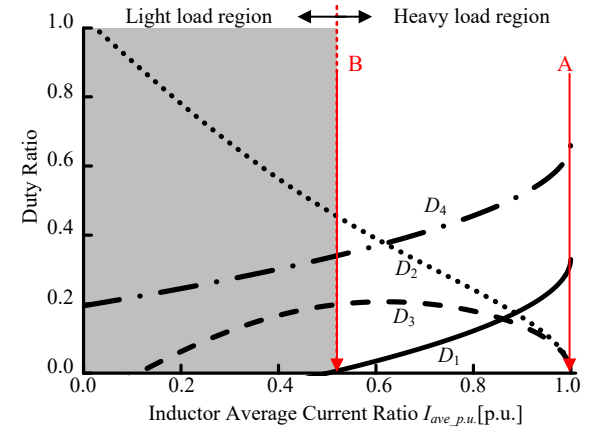


Fig. 5. Inductor current waveform and gate signals of MOSFETs of FCC in rated power for heavy load region.

of the current waveform depends on the voltage conditions and the circuit parameters. Therefore, another switching way for light load region should be considered because this strategy is applied only in heavy load region.

### B. Light load region

Figure 6 shows the inductor current waveform in each switching mode during one switching cycle on heavy load region. Here, the current peak values  $I_{pk2}$  and  $I_{pk3}$  in the respective operation modes are expressed as

$$I_{pk2} = \frac{v_{in} - v_{fc}}{L} D_2 T_{sw} \quad (11),$$

$$I_{pk3} = \frac{v_{in} - v_{dc}}{L} D_4 T_{sw} \quad (12).$$

The slope of the mode II equals to one of the mode III when the flying capacitor voltage  $v_{fc}$  is half of output voltage  $v_{dc}$ . From this,  $D_{23}$  that is sum of the modes II and III period is expressed as

$$D_{23} = D_2 + D_3 = \frac{v_{dc} - v_{in}}{v_{in} - v_{dc} / 2} \quad (13).$$

The sum of the average power in each switching mode equals to the transmission power, which is expressed as

$$\frac{1}{2} I_{pk1} D_1 T_{sw} + \frac{1}{2} I_{pk1} D_{23} T_{sw} = I_{ave} T_{sw} \quad (14).$$

From (11), (12), (13) and (14),  $D_4$  is represented as

$$D_4 = 2 \sqrt{LI_{ave} f_{sw} \frac{v_{in} - v_{dc} / 2}{v_{dc} (v_{dc} - v_{in})}} \quad (15).$$

In FCC, in order to keep the voltage of  $C_{fc}$  constant, the time product of the current flowing through  $C_{fc}$  must be controlled to be zero during one switching period. Therefore, the duties are designed so that the current time products of  $i_L$  in the modes II and III are equal, expressing as

$$\frac{1}{2} (I_{pk1} + I_{pk2}) D_2 T_{sw} - \frac{1}{2} (I_{pk2} + I_{pk3}) D_3 T_{sw} = 0 \quad (16).$$

From (11), (12), (14) and (16),  $D_2, D_3$  is represented as

$$D_2 = \frac{1}{\sqrt{2}} \frac{v_{dc} - v_{in}}{v_{in} - v_{dc} / 2} D_4 \quad (17),$$

$$D_3 = D_{23} - D_2 \quad (18).$$

Figure 7 shows the relationship between the average current and duty ratio  $D_2$ – $D_4$ . As can be seen in Fig. 7, since the sum of the duties are possible to take less than 1, it is confirmed that there are an upper limit value for the value that the average current  $I_{ave}$  is possible to generate. These duty ratio calculations need to be selectively used in the load region.

### C. Flying capacitor voltage control

Figure 8 shows the flying capacitor voltage waveform in each switching mode during one switching cycle. In the previous section, the duty ratio is derived under the assumption of that the flying capacitor  $C_{fc}$  voltage  $v_{fc}$  is kept at half of the DC-link

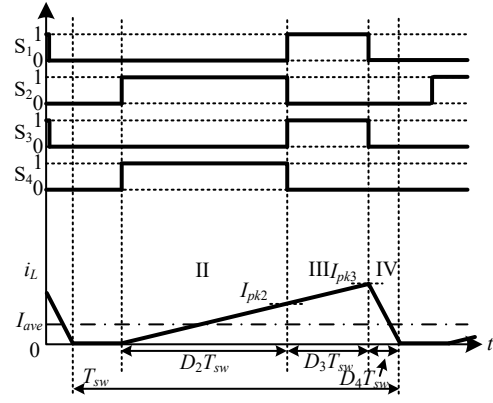


Fig. 6. Inductor current waveform and gate signals of MOSFETs of FCC in rated power for light load region.

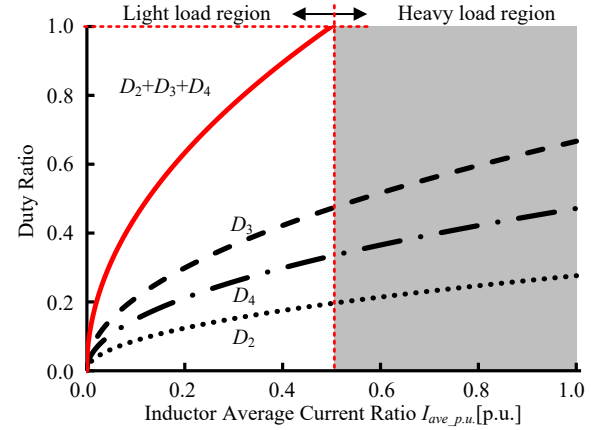


Fig. 7. Relationship between average current and duty for light load region.

voltage. However, the voltage of the flying capacitor varies since the modes II and III charge and discharge the flying capacitor. Furthermore, the inductance information of the boost inductor is required in calculation of the duty ratio however the actual inductance value varies depending on current and heat. Therefore, the flying capacitor voltage may diverge since an error occurs in the duty calculation. Also, Eq. (16) does not satisfy. Therefore, in this paper, feedback control is applied to the flying capacitor voltage.

Figure 9 shows the block diagram of the boost inductor current control and the flying capacitor voltage control system [13]. This controller controls the inductor current and the flying capacitor voltage in two steps. The first step is for calculation of the original duty ratio. The original duty ratio is calculated based on the parameters such as the average inductor current command  $I_{ave}^*$  and the input and output voltage. The second step is for balancing of the flying capacitor voltage. The time ratio of the modes II and III are adjusted by the compensation duty generated by a proportional controller. A voltage command of 1p.u. is input as the command value for a proportional control of flying capacitor voltage. Here, 1p.u. is defined as half of the output voltage. In this control, the flying capacitor voltage  $v_{fc}$  is decreased by an increase in the ratio of the mode II. On the other hand, the flying capacitor voltage  $v_{fc}$  is increased by an increase in the ratio of the mode III. Thus, the flying capacitor voltage is

kept by the control even when the parameter variation of the circuit occurs.

#### IV. EXPERIMENTAL RESULTS

Table I shows the circuit parameters. In this paper, a 200-V single phase grid-tied inverter with a rated power of 1 kW (1p.u.) is assumed as a load.

Figure 10 shows the operation waveforms of high boost ratio. The boost ratio is 3. The current command of each waveform is 0.2p.u. and 1.0p.u.. From Fig. 11, the slope of inductor current in the modes II and III is negative.

Figure 11 shows the operating waveforms of low boost ratio. The boost ratio is 1.5. The current command of each waveform is 0.2p.u. and 1p.u. From Fig. 11, the slope of inductor current in the modes II and III is positive. The input power of 1.0p.u. is in light road region in this boost ratio even though input power is same from the case of high load region. It is confirmed that the boost inductor current  $i_L$  is controlled in a triangular waveform as Fig. 6. Also, the flying capacitor voltage  $v_{fc}$  is keep on half of output voltage  $v_{dc}$ .

Figure 12 and Fig. 13 shows operating waveforms when the power command is changed stepwise from 0.2p.u. to 1p.u., and vice versa. As can be seen from Fig. 12 and 13, the flying capacitor voltage is controlled constant despite the load power fluctuation.

Figure 14 shows the efficiency characteristics. As a result, the maximum efficiency of 98.1% is achieved at an input voltage of 200 V. In this paper, the states of all MOFFETs in Mode IV are all off. Therefore, over all the efficiency becomes better by the synchronous switching is applied.

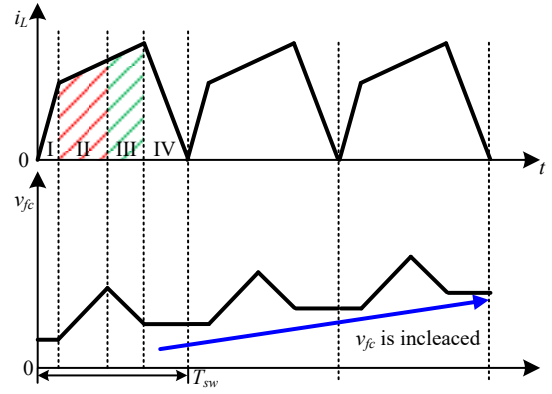
#### V. CONCLUSION

This paper proposed the operation method of DCM applied to inductor current control of FCC for the low boost ratio. The same calculation for each duty ratio is applied in heavy load region. However, the duty calculation for light load region can not applied because the slope of the modes II and III are inverted when boost ratio is less than 2. Therefore, the calculation method of duty ratio is applied for switching pattern without the mode I. Also, the voltage control of frying capacitor is combined for this method.

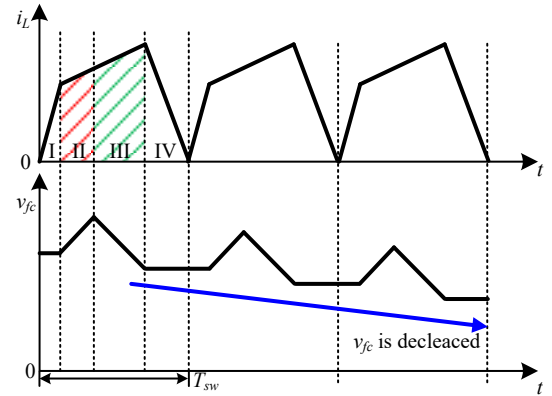
The analysis is verified with a 1-kW prototype. The experimental results show the relevance of this method. The maximum efficiency of 98.1% is achieved at an input voltage of 200 V.

#### REFERENCES

- [1] Jinsoo Han, Jin-Doo Jeong, Ilwoo Lee, Sang-Ha Kim : "Low-cost monitoring of photovoltaic systems at panel level in residential homes based on power line communication" IEEE Trans. on Consumer Electronics, Vol. 63, No. 4, pp. 435–441 (2017)
- [2] Yi Tang, Wenli Yao, Poh Chiang Loh, Frede Blaabjerg : "Highly Reliable Transformers Photovoltaic Inverters With Leakage Current and Pulsating Power Elimination", IEEE Trans. on Industrial Electronics, Vol. 63, No. 2, pp. 1016–1026 (2016)
- [3] T. Shimizu, K. Wada, N. Nakamura : "Flyback-Type Single-Phase Utility Interactive Inverter With Power Pulsation Decoupling on the DC Input



(a)Charging



(b)Discharging

Fig. 8. Flying capacitor voltage change during Mode II and Mode III.

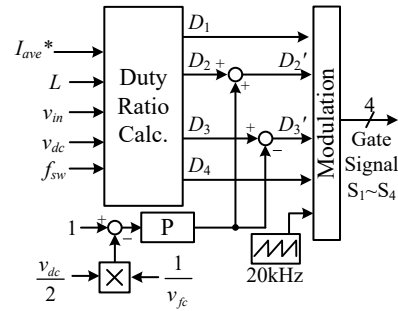


Fig. 9. Block Diagram of flying capacitor converter.

for an AC Photovoltaic Module System", IEEE Trans. on Power Electronics, Vol. 21, No. 5, pp. 1264–1272 (2006)

- [4] Subhendu Dutta, Kishore Chatterjee : "A Buck and Boost Based Grid Connected PV Inverter Maximizing Power Yield From Two PV Arrays in Mismatched Environmental Conditions", IEEE Transactions on Industrial Electronics, Vol. 65, No. 7 (2018)
- [5] Ritwik Chattopadhyay, Subhashish Bhattacharya, Nicole C. Foureaux, Igor A. Pires, Helder de Paula, Lenin Moraes, Porfirio C. Cortizio, Sidelmo M. Silva, Braz Cardoso Filho, and Jose A. de S. Brito, "Low-Voltage PV Power Integration into Medium Voltage Grid Using High-Voltage SiC Devices", IEEJ Journal of Industry Applications, Vol.4, No.6, pp.767–775, (2015)
- [6] Jun Imaoka, Kenkichi Okamoto, Shota Kimura, Mostafa Noah, Wilmar Martinez, Masayoshi Yamamoto, Masahito Shoyama, : "A Magnetic Design Method Considering DC-Biased Magnetization for Integrated Magnetic Components Used in Multiphase Boost Converters", IEEE Trans. on Power Electronics, Vol. 33, No. 4, pp. 3346–3362 (2018)

Table I. Experimental Condition.

Input voltage	$v_{in}$	100V or 200 V
Output voltage	$v_{dc}$	300 V
Switching frequency	$f_{sw}$	20 kHz
Boost inductor	$L$	124 $\mu$ H
Flying Capacitor	$C_{fc}$	60 $\mu$ F, 1200 V *3 Parallel
Switching Devices	$S_1$ - $S_4$	IXFN132N50P3
Gate Resistor		4.7 $\Omega$

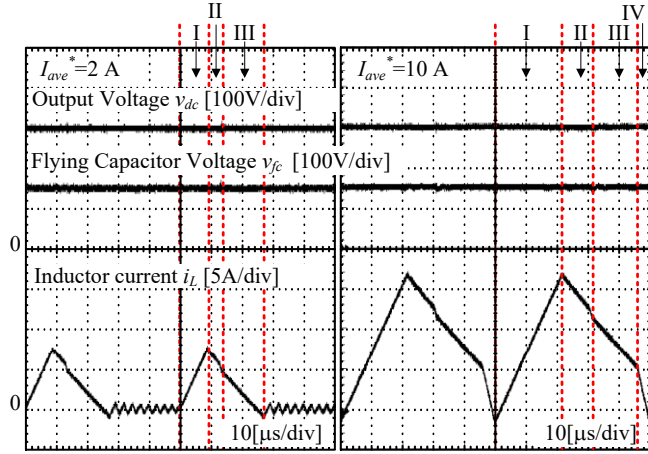


Fig. 10. Operation waveforms of high boost ratio condition.

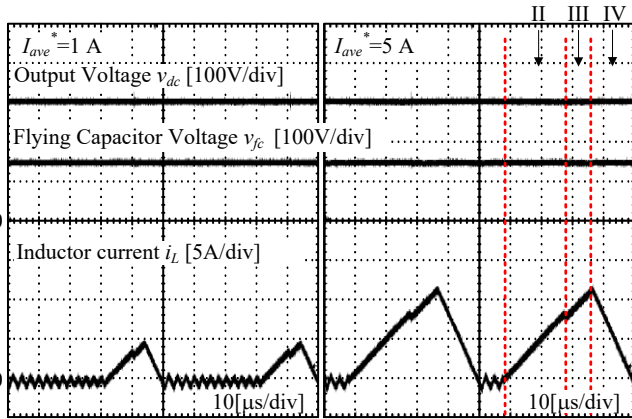


Fig. 11. Operation waveforms of low boost ratio condition.

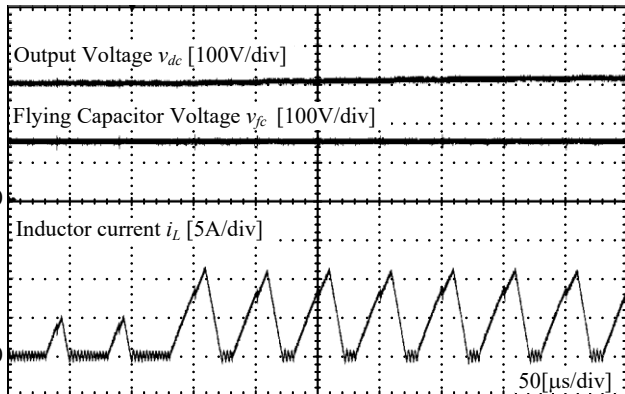


Fig. 12. Operation wave of current step up response.

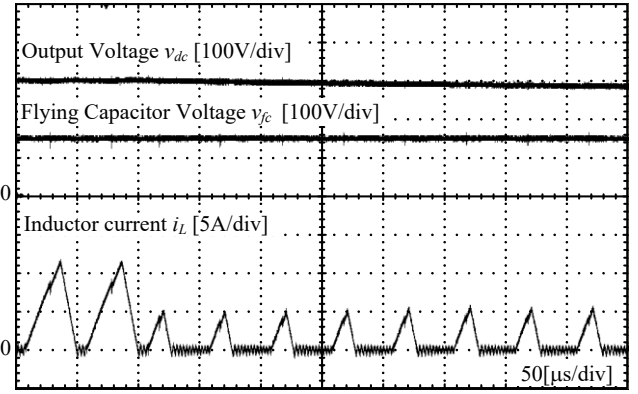


Fig. 13. Operation wave of current step down response.

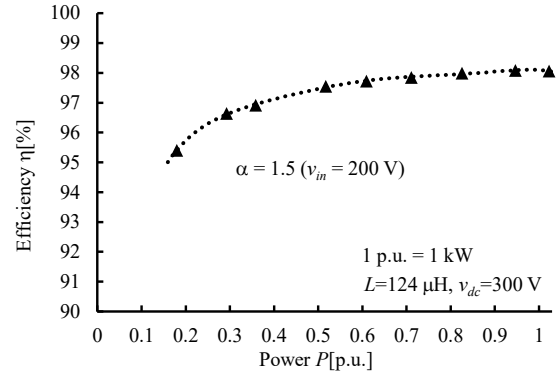


Fig. 14. Efficiency characteristic.

- [7] Gautham Ram, Chandra Mouli, Jos H. Schijffelen, Pavol Bauer, Miroslav Zeman : "Design and Comparison of a 10-kW Interleaved Boost Converter for PV Application Using Si and SiC Devices", IEEE Journal of Emerging and Selected Topics in Power Electronics, Vol. 5, No. 2, pp. 610–623 (2016)
- [8] J. Itoh, T. Aaraki, K. Orikawa: "Experimental Verification of EMC Filter Used for PWM Inverter with Wide Band-Gap Devices", IEEE Journal of Industry Applications, Vol. 4, No. 3, pp. 212–219 (2015)
- [9] H. N. Le, K. Orikawa, J. Itoh : "DCM Control Method of Boost Converter based on Conventional CCM Control", The 2014 International Power Electronics Conference, No. 21A4-5, pp. 3661–3666 (2014)
- [10] Hoai Nam Le, Daisuke Sato, Koji Orikawa, Jun-ichi Itoh : "Efficiency Improvement at Light Load in Bidirectional DC-DC Converter by Utilizing Discontinuous Current Mode", 17th Conference on Power Electronics and Applications, EPE'15-ECCE Europe, No. DS1b-Topic 3-0484, (2015)
- [11] Mahdi Salimi, Abel Zakipour, "Direct Voltage Regulation of DC–DC Buck Converter in a Wide Range of Operation using Adaptive Input-Output Linearization" IEE of Japan Trans. on Electrical and Electronic Engineering, Vol. 10, pp. 85–91 (2015)
- [12] Yasuhiro Sugimoto, Toru Sai, Kei Watanabe, Mikio Abe : "Feedback Loop Analysis and Optimized Compensation Slope of the Current-Mode Buck DC-DC Converter in DCM", IEEE Trans. on Circuits and Systems, Vol. 62, No. 1, p.311–319 (2015)
- [13] R. Ishibashi, H. N. Le, H. Watanabe, K. Kusaka, J. Itoh: "Experimental Verification of Three-level Flying Capacitor Converter Operated in Discontinuous Current Mode", JIASC2018, Vol. , No. 1-29, pp. (2018)(in Japanese)